IEEE Access
Multidisciplinary | Rapid Review | Open Access Journal

Received May 15, 2021, accepted June 4, 2021, date of publication June 16, 2021, date of current version June 23, 2021.

Digital Object Identifier 10.1109/ACCESS.2021.3087543

An Active Voltage Stabilizer for a DC Microgrid System

VISHNU MAHADEVA IYER[1], (Senior Member, IEEE), SRINIVAS GULUR[2], (Member, IEEE), SUBHASHISH BHATTACHARYA[3], (Senior Member, IEEE), JUN KIKUCHI[4], (Member, IEEE), SRIKANTHAN SRIDHARAN[5], KE ZOU[4], AND CHINGCHI CHEN[4]

[1]Department of Electrical Engineering, Indian Institute of Science, Bengaluru 560012, India
[2]Lucid Motors Inc., Newark, CA 94560, USA
[3]Department of ECE, North Carolina State University, Raleigh, NC 27695, USA
[4]FORD Motor Company, Dearborn, MI 48126, USA
[5]Department of Engineering Design, Indian Institute of Technology Madras, Chennai 600036, India

Corresponding author: Vishnu Mahadeva Iyer (vishnumi@iisc.ac.in)

ABSTRACT This paper analyzes the low-frequency stability challenges that exist in a complex DC microgrid (MG) system. The converters that belong to a DC MG are categorized into different groups based on their control approach. The small-signal model of the DC MG is presented, and the conditions for system stability are derived. In some DC MG applications, there is the possibility of installing off-the-shelf converters with little flexibility and access for controller auto-tuning. To tackle this, a hardware-based active voltage stabilizer solution is proposed to stabilize the DC MG. The active stabilizer's functionality, based on an isolated bidirectional DC-DC converter, is elucidated, and a suitable control strategy is proposed. The active stabilizer and its associated control configuration involve only local voltage sensing and are non-intrusive. A dual active bridge (DAB) converter-based active stabilizer is implemented, and hardware-based steady-state and transient experimental results from a DC MG test-bench are provided to validate the functionality and effectiveness of the proposed active stabilizer.

INDEX TERMS Active stabilizer, DC microgrid, dual active bridge (DAB), energy storage, impedance emulation, small signal modeling, small signal impedance, stability.

I. INTRODUCTION

A DC microgrid (MG) offers several inherent advantages over an AC MG. DC MGs require fewer power conversion stages to interface with renewable energy sources and energy storage systems, leading to higher system efficiency [1]. Further, the absence of reactive power and grid voltage harmonics in a DC grid reduces control complexity. With the advent of solid-state transformers, DC MGs are increasingly being used in weight critical applications such as aircraft, marine, and vehicular power conversion systems [2]–[4].

The interactions among different power converters in a DC MG can give rise to system-level stability challenges. These interactions can be analyzed with reasonable accuracy using the small-signal models of power converters if the DC MG voltage is well regulated. However, if the DC MG voltage varies over a wide range, non-linear large-signal modeling techniques are better suited to study these interactions [5], [6]. Different methods have been proposed in the literature to assess multi-converter system stability based on small-signal impedance interactions [7].

Traditionally, the converters in a MG are grouped into the source, and load subsystems [8]–[10]. In [11], an alternate approach is presented wherein the converters in a DC MG are categorized into Bus Voltage Controlled Converters (BVCC) and Bus Current Controlled Converters (BCCC). Examples are presented to represent any DC MG in a general form (with BVCCs and BCCCs) regardless of its structure and operating mode. However, it may not always be intuitive to represent all the converters into these two categories, especially when some converters neither control the bus voltage nor the bus currents.

In this work, an improved grouping approach is proposed to categorize the converters in a DC microgrid. A new converter category called ''Indirect Bus Impedance Converters (IBIC)'' is introduced. The converters in any DC MG are categorized into an BVCCs, BCCCs and IBICs. This approach eliminates the modeling complexity in [11] and helps to come up with

The associate editor coordinating the review of this manuscript and approving it for publication was Zhiwei Gao.

a generalized yet simple small-signal model for the DC MG. Additionally, the proposed grouping approach offers intuitive insights while modeling the converters that share an interlinked control system.

The undesirable impedance interactions among converters can arise due to several reasons. Tightly regulated point of load (POL) converters (DC/DC or DC/AC types) in a DC MG act as constant power loads (CPL) with a negative incremental impedance [12], [13]. In [14], it is shown that converters (DC/AC type) that try to regulate the DC bus voltage can behave as negative incremental impedances with a reversal in the direction of power flow. The negative incremental impedance emulation effect is one of the common reasons for instability as it degrades the system stability margins. The system stability margins can be improved by means of active stabilization. There are two popular approaches to realize the concept of active stabilization - software (or control) based or hardware-based.

The software-based approach necessitates the modification of control loops of one or more converters in the MG to reshape their input or output impedances [12], [15]–[19]. In [20], [21], stabilizing feedback-based methods are presented to ensure global stabilization of a DC MG with multiple converters. Software-based approaches are cost-effective as no external hardware is needed to stabilize the system. Further, one or more of the converters in the DC MG can be used to perform online stability monitoring, and the converter control systems can be adaptively modified to ensure system stability at all times [19], [22]–[25]. In some applications, one or more of the converters in the MG could be off-the-shelf commercial installations. There may not exist any flexibility to modify the control structure of such off-the-shelf converters. This can be tackled by adopting a hardware-based stabilization approach.

In the hardware-based approach, a dedicated power converter-based active stabilizing solution is introduced to stabilize the DC MG. Hardware-based solutions are typically more expensive as compared to software-based solutions. In addition, there will be some losses associated with the power-converter-based stabilizer. The stabilizing power converter can be inserted in series with some of the existing converters in the DC MG [26], [27] or can be added as a shunt element [28]–[30]. Inserting a converter in series requires modification of the connection configurations within the existing MG, while the shunt configuration is less intrusive and is preferred in many applications. In [29], a shunt-type active stabilizer that uses a capacitor-based energy storage system (ESS) is introduced and discussed. In [28], shunt-type battery ESS combined with a power converter is emulated as a smart resistor to actively stabilize a DC MG.

This work presents a shunt-type active stabilizer with a capacitive ESS. The scope of this work is restricted to small-signal model based stability assessment and active stabilization using the proposed stabilizer. An isolated shunt type active stabilizer that utilizes a capacitive ESS and its control was introduced and briefly discussed in the conference version of this work [30]. The key contributions of this article are given below.

- Categorization of the converters in a microgrid into three groups - Group 1 (BVCC), Group 2 (BCCC) and Group 3 (IBIC). The proposed grouping approach yields a simple small-signal model for a DC MG in a generalized form that can be used for small-signal stability assessment using standard time-domain or frequency-domain techniques.
- A hardware based active stabilizer with a novel yet simple single-loop control that uses a capacitor-based ESS. The impedance emulation and active damping effects achieved by the proposed control strategy are elucidated. A design methodology is presented to select the power-stage passive components and control parameters of the proposed active stabilizer.
- Unlike some of the solutions reported in literature [28], [29], it is demonstrated that the proposed active stabilizer achieves stabilization without the need for any high-bandwidth control system or any internal plant model.

Detailed transfer functions are derived to analyze the impact of the emulated impedance (using the active stabilizer and its control system) on the stability of the overall MG DC bus. It is demonstrated that a proportional-integral (PI) type controller can be utilized for emulating an 'R $\parallel$ L + C' type virtual impedance to achieve satisfactory active damping. Experimental results from a DC MG laboratory test-bench are presented to validate the effectiveness of the proposed stabilizer. The proposed active stabilizer does not have to be rated to handle any continuous power. It consumes only minimal power (to meet the losses within the converter) under stable steady-state operating conditions. The proposed solution involves only local voltage sensing and is non-intrusive to any of the existing converters in the DC MG.

The remainder of this article is organized as follows. Section II defines a grouping methodology for the DC MG system under consideration. Section III analyzes the small-signal modeling aspects of the DC MG system. The proposed active stabilizer concept and its control strategy are discussed and analyzed in Section IV. The details of the DC MG test-bench and the active stabilizer parameter selection considerations are discussed in Section V. Detailed experimental results are provided in Section VI. Section VII summarizes the key ideas and concludes this article.

II. DC MICROGRID REPRESENTATION

The structure of the DC MG system considered for this study is presented in Fig. 1. The stability of the DC MG can be assessed by analyzing the dynamics from a linearized model (around a DC operating point) of the power converters. To develop a small-signal model with high fidelity, complete information about the steady-state operating point, as well as the power stage and control stage parameters of individual

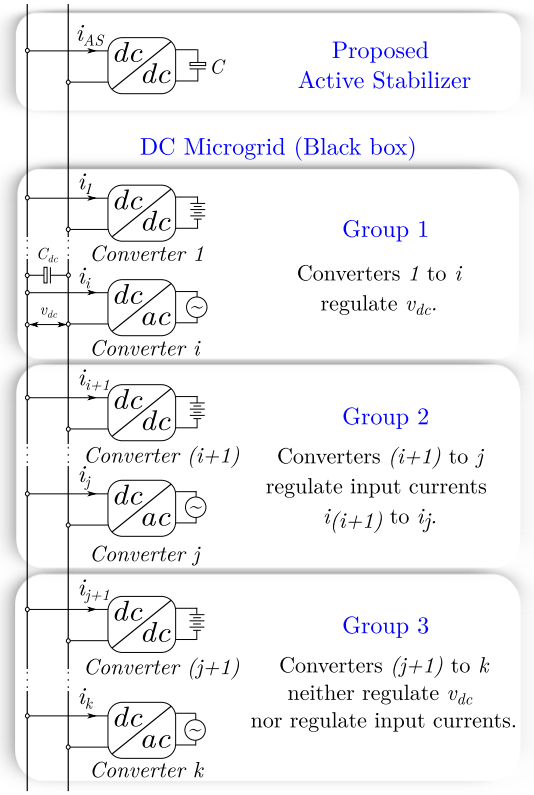

FIGURE 1. Generic DC microgrid with the active stabilizer. The converters in the DC microgrid are categorized into 3 groups.

converters, are essential. In a practical scenario, one may not have access to all the information, and hence, it may not be possible to derive such a high-fidelity small-signal model. However, valuable inferences about system stability can still be obtained from a simpler behavioral model as a first step. Without loss of generality, the converters that belong to this DC MG are broadly grouped into three categories.

1) **Group 1 (BVCC)** - DC-DC converters or DC-AC converters with independent or interlinked control systems that try to regulate the DC voltage of the MG.
2) **Group 2 (BCCC)** - DC-DC converters or DC-AC converters that try to regulate the DC input (MG side) currents.
3) **Group 3 (IBIC)** - DC-DC converters or DC-AC converters that neither control the DC current nor the DC voltage at the MG side belong to this category. Group 3 can include closed-loop converters regulating their output voltage/current/power or regulating their input power. Group 3 can also include converters operating in open-loop.

III. DC MICROGRID MODELING

To analyze the stability of the MG system in which multiple converters share a common DC bus as previously shown in Fig. 1, the interactions between closed-loop unterminated impedances of the individual converters need to be assessed

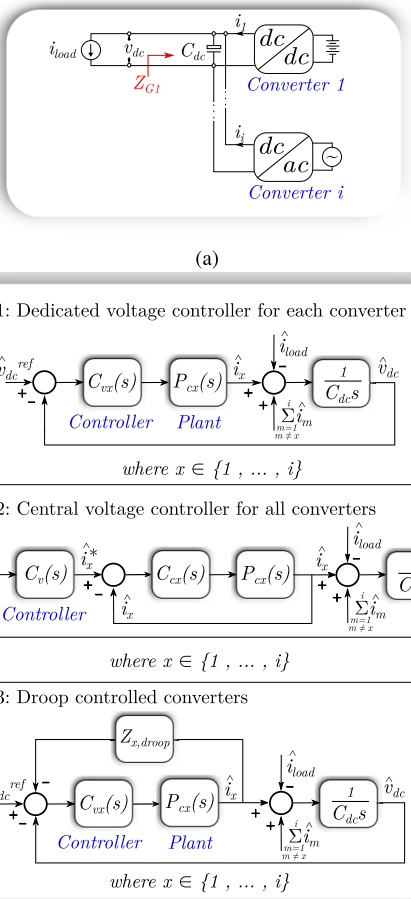

FIGURE 2. Group 1 converters (a) Unterminated representation (b) Small-signal regulator block diagram. $\hat{i}_{load}$ represents a small-signal perturbation in the load current.

[31], [32]. The unterminated representation decouples the converters in a MG from each other.

A. UNTERMINATED MODELING AND SMALL-SIGNAL IMPEDANCES

The unterminated modeling and closed-loop control considerations of converters that belong to each group are discussed separately. The small-signal impedance for each case is evaluated by traditional, well-established block diagram reduction techniques. The details of averaging, linearization, and block diagram reduction techniques can be found in standard textbooks such as [33], [34].

1) GROUP 1 - BUS VOLTAGE CLAMPED CONVERTERS (BVCC)

The unterminated representation of converters pertaining to Group 1 is portrayed in Fig. 2(a). Group 1 converters are a set of paralleled converters that are trying to regulate the DC MG voltage, v_{dc}. The DC bus should be modeled as an ideal current source or a current sink (denoted by i_{load}) as shown in Fig. 2a to decouple the dynamics of other

converters. Broadly, the control approaches for Group 1 converters can be described by three representative cases as depicted in Fig. 2(b). In all the three cases, the control to DC bus current transfer function of x^{th} converter is denoted by $P_{cx}(s)$ where $x \in \{1,\ 2,\ \ldots\ i\}$ as shown in Fig. 2(b) and C_{dc} denotes the DC bus capacitance.

In Case 1, each converter is controlled independently and has a dedicated DC bus voltage controller. The DC bus voltage controller of x^{th} converter is denoted by $C_{vx}(s)$. In this case, the control systems of individual converters will compete with each other, and current sharing cannot be achieved among the paralleled Group 1 converters. Such a control solution is useful only when Group 1 has a single converter that regulates the DC MG voltage.

In Case 2, a central DC bus voltage controller, $C_v(s)$ generates the current references for each of the converters that belong to Group 1 for achieving current sharing as shown in Fig. 2(b). This scheme (with a common DC bus voltage controller) has several variants, and one such variant is the popular 'democratic' current sharing control scheme. Each converter has a dedicated DC current controller, $C_{cx}(s)$ where $x \in \{1,\ 2,\ \ldots\ i\}$.

In Case 3, popular current sharing control scheme for paralleled converters based on droop criteria (and its variants) is used as shown in Fig. 2(b). Each converter has a dedicated DC bus voltage controller, $C_{vx}(s)$ where $x \in \{1,\ 2,\ \ldots\ i\}$. The DC current, i_x is fed back through a droop resistance, $Z_{x,droop}(s)$ for achieving current sharing among the paralleled converters.

From these examples, the DC bus impedance of Group 1 converters with independent or interlinked control systems can be generically represented as

$$Z_{G1}(s) = \frac{\hat{v}_{dc}(s)}{\hat{i}_{load}(s)} = \frac{1}{\frac{1}{Z_c(s)} + \frac{1}{Z_{CL}(s)}} \tag{1}$$

$$Z_{CL}(s) = \begin{cases} \dfrac{1}{\sum\limits_{x=1}^{i} C_{vx}(s)P_{cx}(s)} & (Case\ 1) \\ \dfrac{1}{C_v(s)\sum\limits_{x=1}^{i} \dfrac{C_{cx}(s)P_{cx}(s)}{1 + C_{cx}(s)P_{cx}(s)}} & (Case\ 2) \\ \dfrac{1 + \sum\limits_{x=1}^{i} C_{vx}(s)P_{cx}(s)Z_{x,droop}(s)}{\sum\limits_{x=1}^{i} C_{vx}(s)P_{cx}(s)} & (Case\ 3) \end{cases} \tag{2}$$

where $Z_c(s) = \dfrac{1}{sC_{dc}}$ and $Z_{CL}(s)$ represents the impedance dynamics introduced by the closed loop control system. From (1), it is evident that the effective impedance of Group 1 converters is nothing more than the parallel combination of the DC bus capacitor impedance and the impedance dynamics introduced by the closed loop control system.

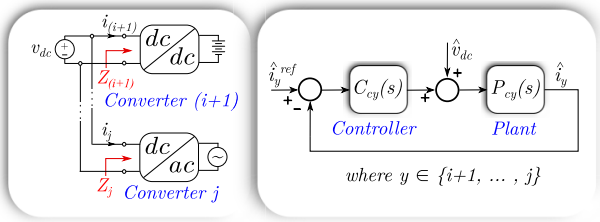

(a) (b)

FIGURE 3. Group 2 converters (a) Unterminated representation (b) Small-signal regulator block diagram.

2) GROUP 2 - BUS CURRENT CLAMPED CONVERTERS (BCCC)

The unterminated representation of converters pertaining to Group 2 as well as their typical control systems are portrayed in Fig. 3(a). Group 2 converters are a set of input-paralleled converters that are trying to regulate their respective input currents referred to the DC MG bus. Each converter is controlled independently and has its own dedicated DC bus current controller, $C_{cy}(s)$ as shown in Fig. 3(b). The control to DC bus current transfer function of y^{th} converter is denoted by $P_{cy}(s)$ where $y \in \{i+1,\ i+2,\ \ldots\ j\}$. In order to decouple the dynamics of other converters, the DC bus seen by Group 2 converters is treated as an ideal DC voltage source as shown in Fig. 3(a). The closed-loop small-signal impedance of y^{th} converter referred to the DC bus, $Z_y(s)$, can be evaluated as

$$Z_y(s) = \frac{\hat{v}_{dc}(s)}{\hat{i}_y(s)} = \frac{1 + C_{cy}(s)P_{cy}(s)}{P_{cy}(s)} \tag{3}$$

where $y \in \{i+1,\ i+2,\ \ldots\ j\}$.

3) GROUP 3 - INDIRECT BUS IMPEDANCE CONVERTERS (IBIC)

The unterminated representation of converters pertaining to Group 3 as well as their typical control systems are portrayed in Fig. 4. Group 3 converters are a set of input-paralleled converters that are neither trying to regulate the DC bus voltage nor regulate their respective input currents referred to the DC bus. The unterminated modeling of Group 3 converters are similar to that of Group 2 converters. The DC MG is treated as an ideal DC voltage source as shown in Fig. 4(a) to decouple the dynamics of other converters. The small-signal closed-loop control representation is depicted in Fig. 4(b). C_z and P_z denote the controller and plant transfer fuctions of the z^{th} converter where $z \in \{j+1,\ j+2,\ \ldots\ k\}$. The effect of DC bus voltage is modeled as a disturbance that acts through the transfer function, G_z. The closed-loop small-signal impedance, $Z_z(s)$ of z^{th} converter referred to the DC bus can be evaluated as in [33].

$$\frac{1}{Z_z(s)} = \frac{1}{Z_N(s)}\left[\frac{L_z(s)}{1 + L_z(s)}\right] + \frac{1}{Z_D(s)}\left[\frac{1}{1 + L_z(s)}\right] \tag{4}$$

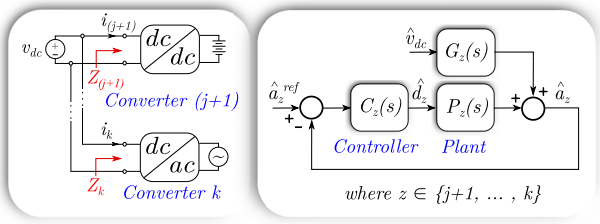

(a) (b)

FIGURE 4. Group 3 converters (a) Unterminated representation (b) Small-signal regulator block diagram. $\hat{a}_z$ can be any quantity other than the voltage or current referred to the DC bus side. Group 3 may also include converters that are operating in open-loop.

where $z \in \{j+1,\ j+2,\ \ldots\ k\}$. $Z_D(s)$ and $Z_N(s)$ are the driving point impedance and null driving point impedance as defined in [33]. $L_z(s)$ denotes the controller loop gain such that $L_z(s) = C_z(s)P_z(s)$.

The control systems provided in Fig. 2(b), Fig. 3(b) and Fig. 4(b) are representative of more complicated practical scenarios. In practical MGs, converter controls may be interlinked (Group 1 converters) or independent (Group 2 or Group 3 converters). The intention here is to demonstrate that any complicated control structure can be finally broken down into one of the three basic forms (Group 1, 2, or 3). A unique small-signal impedance can thus be derived for each converter in Group 2 and Group 3, and an effective small-signal impedance can be derived for all the converters that belong to Group 1.

B. SMALL-SIGNAL MODEL FOR THE DC MICROGRID

The small-signal impedances (referred to the DC bus) for the unterminated converter systems in the DC MG are evaluated as in (1) - (4). Even without the knowledge of any converter-specific parameters, the generic small-signal impedance-based representation of the DC MG can be depicted as in Fig. 5.

All converters that belong to Group 1 (BVCC) try to regulate the DC MG voltage, and their control systems can be modeled as a single Thevenin equivalent. Each converter in Group 2 (BCCC) tries to regulate the current at the DC MG port, and their control system can be modeled as a Norton equivalent. Group 3 (IBIC) converters (open-loop or closed-loop) can be modeled as impedances. All the impedances shown in Fig. 5 correspond to closed-loop small-signal impedances evaluated at the DC port of the unterminated systems as represented in Fig. 2(a), Fig. 3(a) and Fig. 4(a).

It is to be noted that multiple equivalent small-signal representations exist. The Thevenin equivalent depicted in Fig. 5 can be transformed into a Norton equivalent and vice versa. The small-signal model presented in Fig. 5 is just one of the feasible representations. The model depicted in Fig. 5 is tied intuitively to how the individual converters in the DC MG are controlled.

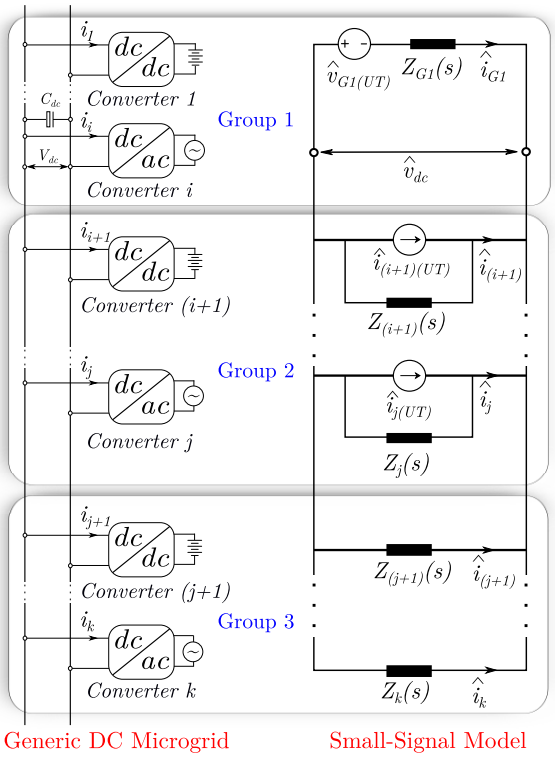

FIGURE 5. Small-signal model of the DC microgrid.

The small-signal DC MG voltage can be evaluated from Fig. 5 as

$$\hat{v}_{dc}(s) = \hat{v}_{G1(UT)}(s) \times \frac{1}{\left[1 + \dfrac{Z_{G1}(s)}{Z_{eq}(s)}\right]} + \left(\hat{i}_{(i+1)(UT)}(s) + \ \ldots\ + \hat{i}_{j(UT)}(s)\right) Z_{bus}(s) \tag{5}$$

$$Z_{eq}(s) = \frac{1}{\sum_{m=i+1}^{k} \dfrac{1}{Z_m(s)}},\ Z_{bus}(s) = \frac{1}{\dfrac{1}{Z_{G1}(s)} + \dfrac{1}{Z_{eq}(s)}} \tag{6}$$

For determining the stability of the generic DC MG system presented in Fig. 1, the following conditions need to be evaluated from (5).

1) Stability of unterminated controlled voltage source, $\hat{v}_{G1(UT)}(s)$.
2) Stability of unterminated controlled current sources, $\hat{i}_{(i+1)(UT)}(s),\ \ldots\ , \hat{i}_{j(UT)}(s)$.
3) Stability of the term $\dfrac{1}{1 + \dfrac{Z_{G1}(s)}{Z_{eq}(s)}}$, where $\dfrac{Z_{G1}(s)}{Z_{eq}(s)}$ is typically referred to as the minor loop gain.
4) Stability of the term $Z_{bus}(s)$.

The 1^{st} and the 2^{nd} conditions imply that the unterminated converters that belong to Group 1 and Group 2 must be internally stable under closed-loop operation. Conditions 3 and 4 are referred to as minor loop gain criterion and passivity criterion respectively in popular literature [7]. Both these

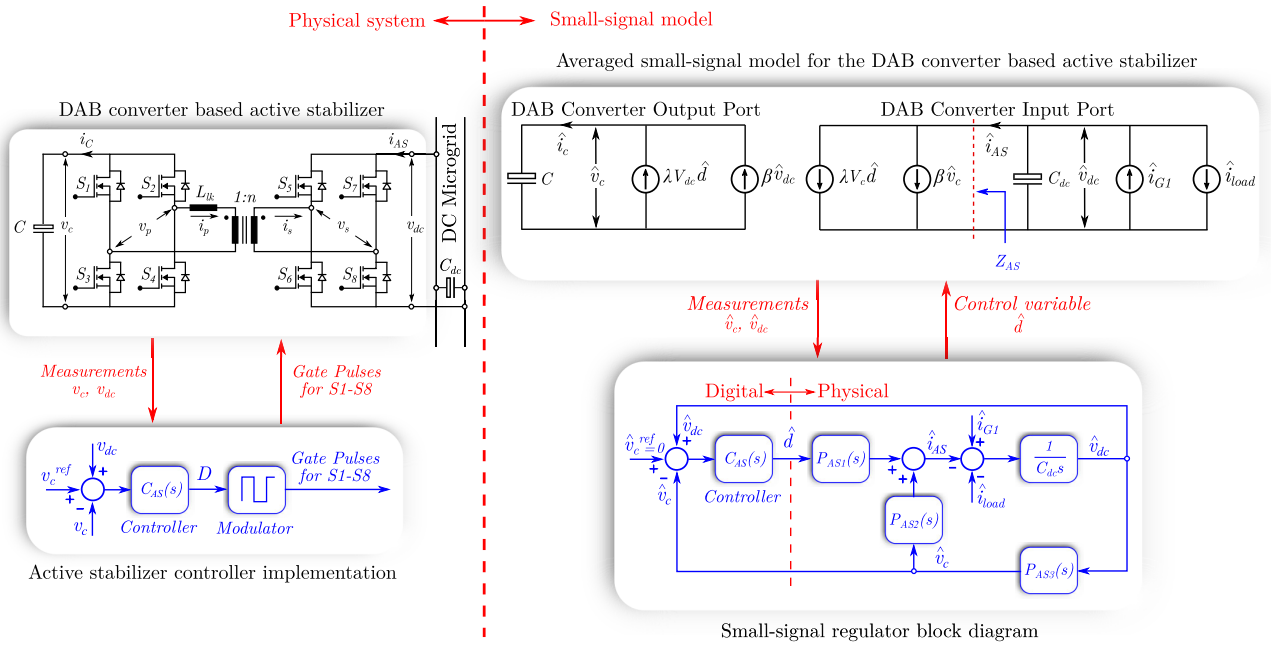

FIGURE 6. DAB converter based active stabilizer realization and its averaged small-signal model.

expressions, $\dfrac{1}{1+\dfrac{Z_{G1}(s)}{Z_{eq(s)}}}$ and Z_{bus}, have identical poles and can hence be interchangeably used for stability assessment.

These conditions reveal that the root cause of DC bus voltage instability in a generic DC MG is the undesirable small-signal impedance interactions of converters in Group 1 with the small-signal impedances of converters that belong to any of the other groups (Group 2 and Group 3). The presence of negative incremental impedances that can lead to instability has been observed in Group 1 converters [14] and Group 3 converters [12], [13]. At the same time, such a negative incremental impedance effect is absent in converters that belong to Group 2 due to DC bus current regulation. All DC MG systems where a DC bus voltage instability has been reported involve at least one or more converters that belong to either Group 1 or Group 3. This observation served as a motivation for the proposed grouping methodology.

IV. PROPOSED ACTIVE VOLTAGE STABILIZER

The proposed active stabilizer solution and its associated control strategy is depicted in Fig. 6. A DAB converter is used to interface a capacitive energy storage system to the DC MG. To understand the DAB converter's operation, modeling, and control aspects, an interested reader is referred to [35]–[37].

Under steady-state conditions, the DC MG voltage is regulated by one or more converters from Group 1. The active stabilizer input capacitor voltage, v_c tracks the DC MG voltage, v_{dc} if $\hat{v}_c^{ref}$ is set to zero. The active stabilizer goes into an idling mode where no power exchange takes place with the MG. Under transient conditions, $v_c \neq v_{dc}$ and the active stabilizer control loop will get activated.

A. ACTIVE STABILIZER OPERATION

The small-signal models for a phase-shift modulated DAB converter based on [14] is used in this work. The relevant transfer functions for the DAB converter-based active stabilizer control system are computed. The transfer functions, $P_{AS1}(s)$ and $P_{AS2}(s)$ can be obtained by inspection from the small-signal model of DAB converter based active stabilizer in Fig. 6. Let V_c and V_{dc} be the averaged DC voltages at the input and output ports of the active stabilizer.

$$P_{AS1}(s) = \frac{\hat{i}_{AS1}(s)}{\hat{d}(s)} = \lambda V_c \tag{7}$$

$$P_{AS2}(s) = \frac{\hat{i}_{AS2}(s)}{\hat{v}_c(s)} = \beta \tag{8}$$

In order to find the tracking transfer function, $P_{AS3}(s)$, the relationship between $\hat{v}_c(s)$ and $\hat{v}_{dc}(s)$ has to be established.

$$\hat{v}_c(s) = (\lambda V_{dc}\hat{d} + \beta\hat{v}_{dc}(s))Z_{cAS}(s) \tag{9}$$

$$\hat{d} = (\hat{v}_{dc}(s) - \hat{v}_c(s))C_{AS}(s) \tag{10}$$

From (9) and (10), $P_{AS3}(s)$ can be evaluated as

$$P_{AS3}(s) = \frac{\hat{v}_c(s)}{\hat{v}_{dc}(s)} = \frac{\big(\beta + C_{AS}(s)\lambda V_{dc}\big)Z_{cAS}(s)}{1 + C_{AS}(s)\lambda V_{dc}Z_{cAS}(s)} \tag{11}$$

where $\beta = \dfrac{T_s}{2nL_{lk}}D(1-|D|)$, $\lambda = \dfrac{T_s}{2nL_{lk}}(1-2|D|)$ and $D = \phi/\pi$, $-\pi/2 < \phi < \pi/2$ as defined in [14]. ϕ is the phase-shift between the bridge voltages, T_s is the switching time period, n is the transformer turns-ratio and L_{lk} is the power transfer inductance of the DAB converter.

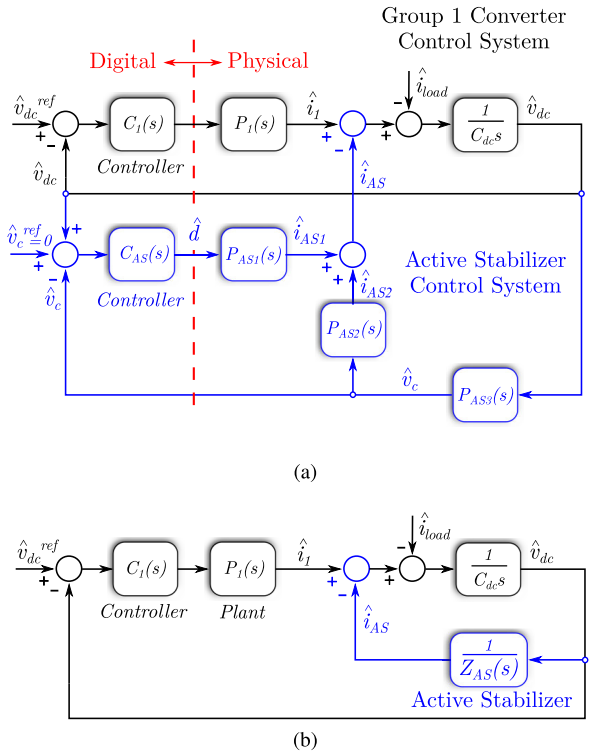

FIGURE 7. (a) Effect of active stabilizer on Group 1 converter control system (b) Simplified representation to showcase effect of active stabilizer.

$Z_{cAS}(s) = 1/(sC)$. A proportional-integral type controller, $C_{AS}(s) = K_p + K_i/s$, is used as the active stabilizer controller.

The proposed control approach stabilizes the DC MG by actively modifying the impedances associated with Group 1 converters that are responsible for MG voltage regulation. The effect of proposed active stabilizer on the Group 1 converter control system is depicted in Fig. 7(a). Fig. 7(a) can be further simplified using block diagram reduction techniques to get From Fig. 7(b). From Fig. 7(b), it can be seen that the active stabilizer emulates a small signal impedance, $Z_{AS}(s)$ that comes in parallel with the DC bus capacitance, C_{dc}. The modified impedance associated with Group 1 converters, $Z_{G1new}(s)$ can now be defined as

$$Z_{G1new}(s) = \frac{1}{\frac{1}{Z_c(s)} + \frac{1}{Z_{CL}(s)} + \frac{1}{Z_{AS}(s)}} \tag{12}$$

where $Z_c(s) = \frac{1}{sC_{dc}}$, $Z_{CL}(s)$ is the impedance dynamics introduced by Group 1 converter control system as in (2), and $Z_{AS}(s)$ is the impedance dynamics introduced by the active stabilizer control system.

$$Z_{AS}(s) = \frac{1}{[1 - P_{AS3}(s)]C_{AS}(s)P_{AS1}(s) + P_{AS2}(s)P_{AS3}(s)} \tag{13}$$

Hence, it can be concluded that the addition of active stabilizer alters the closed-loop small signal impedance associated with Group 1 converters and in turn affects the overall DC bus small signal impedance, $Z_{bus}(s)$. The modified DC bus small signal impedance, $Z_{busnew}(s)$ is given by

$$Z_{busnew}(s) = \frac{1}{\frac{1}{Z_{G1new}(s)} + \frac{1}{Z_{eq}(s)}} \tag{14}$$

The modified minor loop gain, $T_{Gnew}(s)$ is given by

$$T_{Gnew}(s) = \frac{Z_{G1new}(s)}{Z_{eq}(s)} \tag{15}$$

The proposed active stabilizer can be interfaced to any DC MG as in Fig. 1 to improve its stability, provided the MG DC voltage is regulated by one or more converters that belong to Group 1.

B. IMPEDANCE EMULATION AND ACTIVE DAMPING

The emulated impedance transfer function, $Z_{AS}(s)$, can be expanded and represented as follows.

$$Z_{AS}(s) = \frac{\frac{1}{K_p\lambda V_{dc}}\left(\frac{C}{K_i\lambda V_{dc}}s^2 + \frac{K_p}{K_i}s + 1\right)}{\frac{C}{K_i\lambda V_{dc}}s^2 + \left[\frac{C}{K_p\lambda V_{dc}} + \frac{\beta^2}{K_iK_p\lambda^2V_{dc}^2}\right]s} \tag{16}$$

If the parameters are chosen such that $\frac{\beta^2}{K_iK_p\lambda^2 V_{dc}^2} \ll \frac{C}{K_p\lambda V_{dc}}$, then the impedance expression can be approximated as

$$Z_{AS}(s) \approx \frac{\frac{1}{K_p\lambda V_{dc}}\left(\frac{C}{K_i\lambda V_{dc}}s^2 + \frac{K_p}{K_i}s + 1\right)}{\frac{C}{K_i\lambda V_{dc}}s^2 + \frac{C}{K_p\lambda V_{dc}}s} \tag{17}$$

From (17), it can be discerned that the emulated impedance, $Z_{AS}(s)$ behaves like a damped LC network as represented in Fig. 8. The impedance expression for the damped LC network is given in (18).

$$Z_{LCR}(s) = \frac{R_{eq}\left(L_{eq}C_{eq}s^2 + \frac{L_{eq}}{R_{eq}}s + 1\right)}{L_{eq}C_{eq}s^2 + R_{eq}C_{eq}s} \tag{18}$$

By equating the coefficients of individual terms in (17) and (18), the circuit parameters can be identified as follows.

$$L_{eq} = \frac{1}{K_i\lambda V_{dc}},\ C_{eq} = C \quad and \quad R_{eq} = \frac{1}{K_p\lambda V_{dc}} \tag{19}$$

The emulated inductance, L_{eq}, and the emulated resistance, R_{eq}, are inherently adaptive as they are dependent on λ, which is in-turn affected by the power fluctuations handled by the stabilizer. The emulated capacitance, C_{eq}, is non-adaptive. The power-stage parameters of the active stabilizer can be chosen to minimize the influence of power fluctuations on the emulated impedance. The emulated inductance, L_{eq} can be tuned by varying K_i, the emulated resistance, R_{eq} can be tuned by varying K_p and the emulated capacitance, C_{eq} can be tuned by varying C. This approach offers the flexibility

TABLE 1. Comparison of proposed approach with other popular hardware-based active stabilizer approaches.

Approach	Type	ESS	No. of Sensors	No. of Controllers	Constraint on ESS Voltage	Bandwidth Requirement	Galvanic Isolation	Ground Fault Immunity	Control Complexity
Hosseinipour et. al [27]	Series	Battery	2	3	$V_{ESS} > V_{dc}$	High	No	No	Medium
Potty et.al [28]	Shunt	Battery	3	3	$V_{ESS} > V_{dc}$	High	No	No	Medium
Zhang et.al [29]	Shunt	Capacitor	3	3	$V_{ESS} > V_{dc}$	High	No	No	High
Proposed (this work)	Shunt	Capacitor	2	1	$V_{ESS} > 0$	Low	Yes	Yes	Low

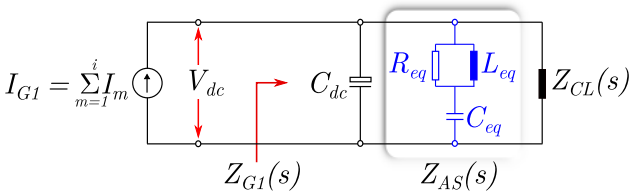

FIGURE 8. Equivalent circuit representation to showcase the effect of active stabilizer on Group 1 converters.

to independently tune each element (L_{eq}, C_{eq} or R_{eq}) by selecting the power stage and control parameters (C, K_p or K_i) to achieve a desired impedance to stabilize the DC MG. It is interesting to note that as $R_{eq} \rightarrow \infty$ (or $K_p \rightarrow 0$), the emulated impedance behaves like a series LC circuit while when $L_{eq} \rightarrow \infty$ (or $K_i \rightarrow 0$), the emulated impedance behaves like a series RC circuit.

C. NEED FOR GALVANIC ISOLATION

It is critical to discuss the grounding strategies used in a typical DC MG to understand the need for galvanic isolation within the active stabilizer. IEC 60364-1 discusses three basic grounding strategies for a DC MG - Terre-Neutral (TN), Terre-Terre (TT), and Isolé-Terre (IT) [38]. In TN systems, one of the line conductors is directly connected to the ground. Based on how the grounded line and protective conductors are fed, there are further sub-classifications to the TN system. TT systems have one line conductor directly connected to the ground. Further, all exposed conductive parts of the installation will be grounded using earth electrodes. In IT systems, the installation is either insulated from the ground or connected to the ground through a sufficiently high impedance. All exposed conductive parts of the installation will be grounded using earth electrodes.

A scenario where one of the line conductors of the DC MG is solidly grounded is depicted in Fig. 9. Further, Fig. 9 showcases a ground fault condition within the active stabilizer connected to such a DC MG. If a non-isolated active stabilizer such as the one presented in [29] is used as in Fig. 9(a), the capacitive energy storage device can drive large transient currents into the ground under a low impedance ground fault condition. The ground-fault current could trip the residual current device (RCD) that is typically used to protect the DC MG against ground faults. Any fault within the active stabilizer can thus potentially trip the entire DC MG. To prevent tripping the entire MG, a Dual Active Bridge (DAB) based converter with inbuilt galvanic isolation, as in Fig. 9(b), is proposed. Even if a ground fault occurs within the active stabilizer, the capacitive energy storage device cannot feed any fault current in this case. The proposed isolated active stabilizer can be used with any DC MG irrespective of the grounding scheme. Non-isolated active stabilizers, as in [29] could be potentially used for DC MGs with an IT grounding scheme.

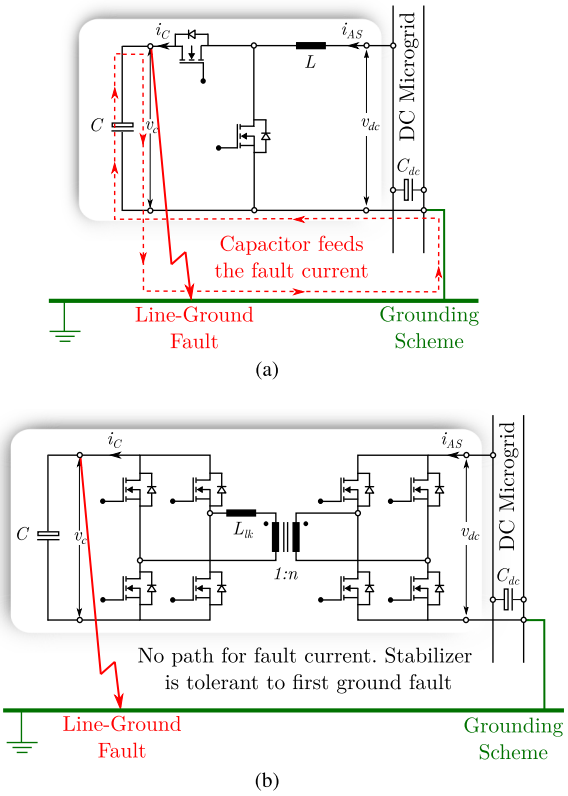

FIGURE 9. Ground fault scenario for a solidly grounded DC microgrid with (a) non-isolated active stabilizer [29] (b) proposed isolated active stabilizer.

D. COMPARISON WITH POPULAR APPROACHES

The proposed approach is compared with some of the popular hardware-based active stabilizer approaches in Table. 1 to highlight the key differences. The proposed approach utilizes a simple single-loop control structure with fewer sensing requirements. There is no need to implement any internal plant model as in [29], and there is no high bandwidth requirement as in [28]. Further, the isolated DAB topology

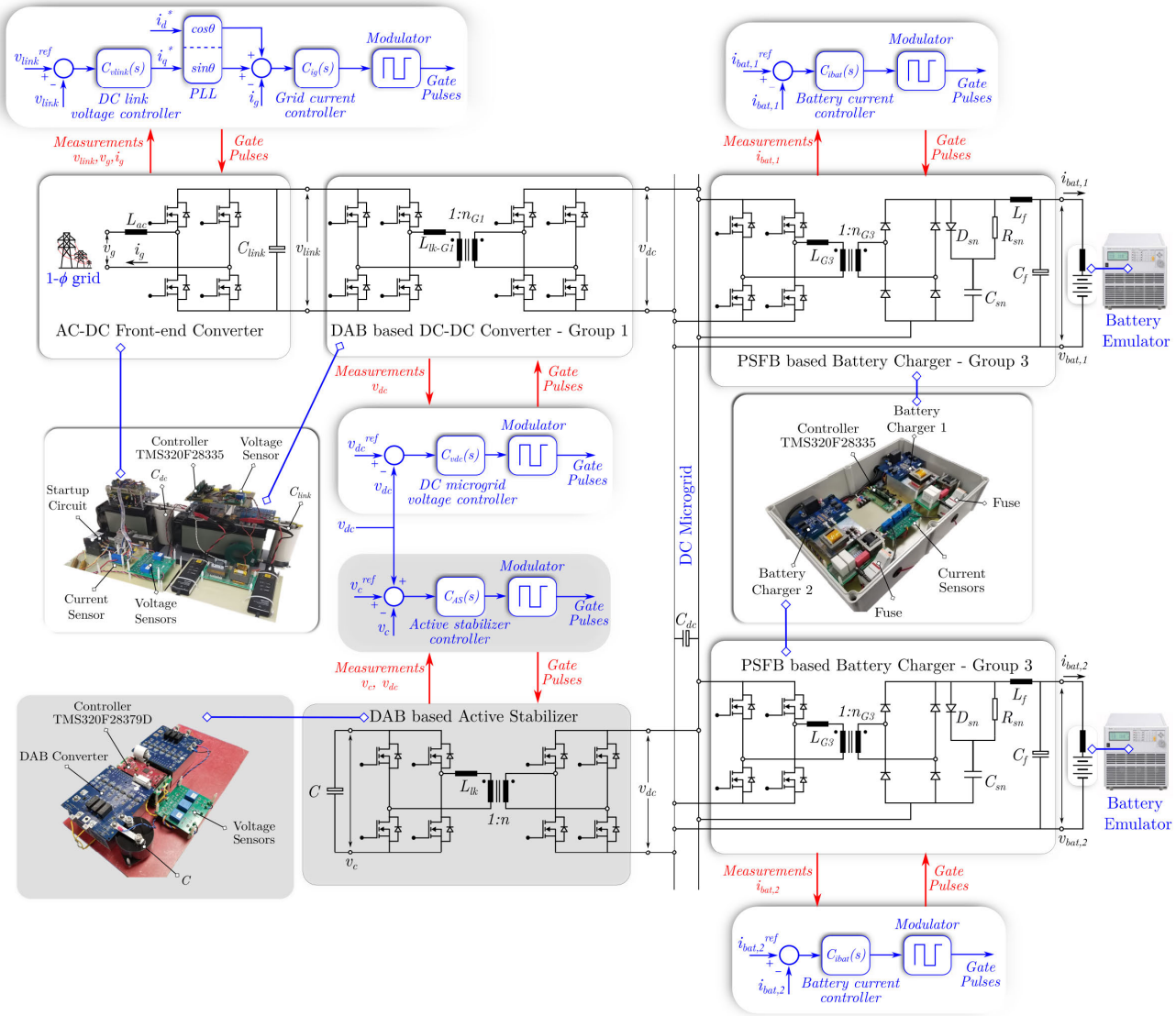

FIGURE 10. Experimental DC microgrid test-bench in the laboratory with the proposed active stabilizer. Closed loop control realization for each converter is depicted.

offers immunity to the first ground fault as opposed to the approaches discussed in literature [28], [29].

V. DC MICROGRID TESTBENCH

A DC MG hardware test bench has been developed in the laboratory, as shown in Fig. 10 to validate the effectiveness of the proposed active stabilizer and its associated control strategy.

A. GROUPING AND IMPEDANCE INTERACTIONS

A grid interfaced power conversion stage, that comprises of a single-phase AC-DC converter cascaded with a DAB based DC-DC converter, regulates the DC MG voltage to 300 V. As per the grouping methodology presented in Section II, the DAB converter falls under Group 1 since it directly regulates the DC MG voltage. Two DC-DC power conversion units, based on the Phase-Shifted Full Bridge (PSFB) Pulse Width Modulated (PWM) converter, have been interfaced to the DC MG. These converters are configured to facilitate battery charging by means of partial power processing. As the PSFB converters neither directly control the DC MG voltage nor the DC MG current, they fall under Group 3 category. Finally, a DAB converter-based active stabilizer as discussed in Section IV is interfaced with the DC MG. The relevant circuit and control parameters of the converters in the DC MG are listed in Table. 2. An interested reader is referred to [14] and [39] for details on modeling the various converters that are being used in the presented DC MG. The small-signal impedances of each converter, as seen from the DC MG, can be evaluated based on the methodology presented in Sec. III.

The small-signal unterminated impedance plots of the converters that belong to different groups are presented in Fig. 11(a). The accuracy of the analytical impedance models are validated by performing a small-signal analysis

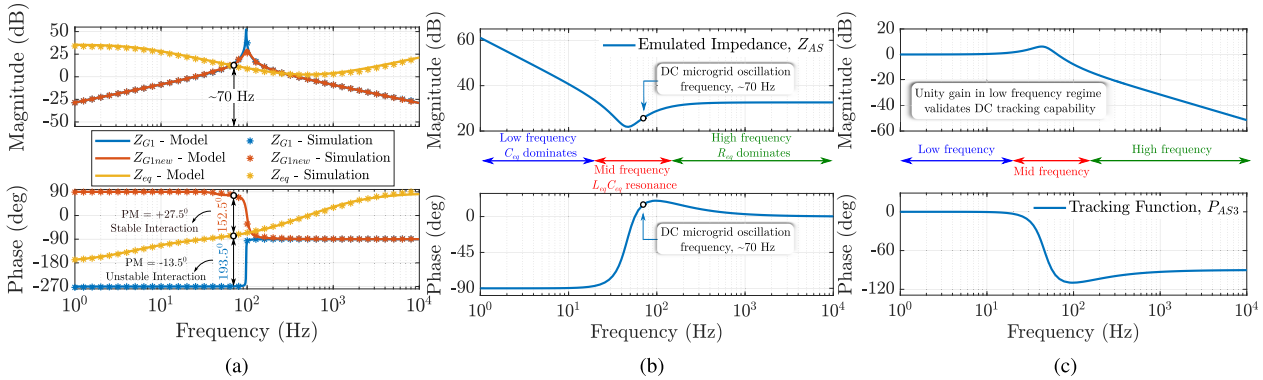

FIGURE 11. Frequency response plots (a) small-signal impedance interaction that can cause instability is avoided with the use of active stabilizer. $Z_{G1}(s)$ and $Z_{G1new}(s)$ refer to the impedance of Group 1 converter without and with active stabilizer. The accuracy of the analytical model is validated by performing small-signal analysis on the switching circuit simulation. (b) Small-signal impedance, $Z_{AS}(s)$ emulated by the active stabilizer (c) Tracking function, $P_{AS3}(s) = \frac{\hat{v}_C(s)}{\hat{v}_{dc}(s)}$ to showcase DC tracking capabilities.

TABLE 2. Experimental test bench parameters.

Grid Tied AC-DC Front-end Converter	
AC filter inductance, L_{ac}	$1\ mH$
DC bus capacitance, C_{link}	$450\ \mu F$
Switching frequency, $f_{sw(AC-DC)}$	$20\ kHz$
Fundamental frequency, f_g	$\approx 60\ Hz$
AC input voltage, v_g	$200\ V(rms)$
DC output voltage, v_{link}	$400\ V$
DC link voltage controller, $C_{vlink}(s)$	$0.05 + 10/s$
Grid current controller, $C_{ig}(s)$	$0.03 + \frac{12.5s}{s^2 + (2\pi \times 60)^2}$
Dual Active Bridge (DAB) based DC-DC Converter	
Inductance, L_{lk-G1}	$64\ \mu H$
Transformer turns ratio, n_{G1}	1.0
DC bus capacitance, C_{dc}	$450\ \mu F$
Switching frequency, $f_{sw(DC-DC)}$	$50\ kHz$
DC microgrid voltage, v_{dc}	$300\ V$
DC microgrid voltage controller, $C_{vdc}(s)$	$0.00002 + 3.5/s$
Phase-Shifted Full Bridge (PSFB) based Battery Chargers	
Leakage inductance, L_{lk-G3}	$11\ \mu H$
Transformer turns ratio, n_{G3}	0.35
Filter inductance, L_f	$520\ \mu H$
Filter capacitance, C_f	$20\ \mu F$
Switching frequency, $f_{sw(Charger)}$	$50\ kHz$
Battery voltage, $v_{bat,i}\vert_{i\in\{1,2\}}$	$360 - 400\ V$
Battery current controller, $C_{ibat}(s)$	$0.02975 + 50/s$
Dual Active Bridge (DAB) based Active Stabilizer	
Capacitor voltage, v_c	300 V
Capacitance, C	$140\ \mu F$
Inductance, L_{lk}	$64\ \mu H$
Turns ratio, n	1.0
Switching frequency, $f_{sw(AS)}$	50 kHz
Active stabilizer controller, $C_{AS}(s)$	$0.0005 + 0.25/s$

on the switching circuit simulation of the converters in the MG as shown in Fig. 11(a). The small-signal model validation was performed using the circuit simulation platform, 'PLECS' [40]. In the absence of the proposed active stabilizer, undesirable small-signal impedance interaction is observed around 70 Hz between Group 1 converter ($Z_{G1}(s)$) and Group 3 converters ($Z_{eq}(s)$) resulting in a negative phase-margin (-13.5^0). The small-signal impedance of Group 1 converter ($Z_{G1new}(s)$) is modified when the active

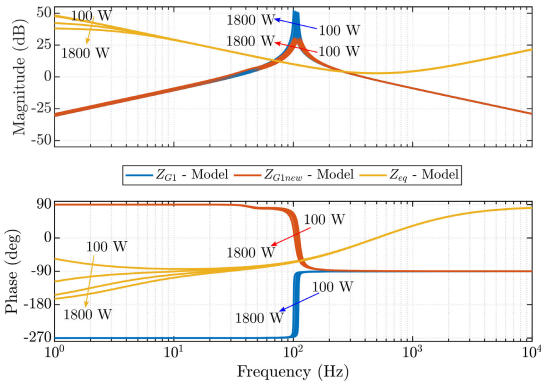

FIGURE 12. Effect of load variation on converter impedances.

stabilizer is introduced. The phase-margin improves to 27.5^0. Further, the small-signal impedance emulated by the active stabilizer, $Z_{AS}(s)$, is plotted in Fig. 11(b). It can be seen that the resonance in the emulated small-signal impedance falls below the frequency of undesired oscillations. The emulated small-signal impedance behaves like a capacitor in the low-frequency regime and as a resistor in the high-frequency regime. Finally, to ensure that the active stabilizer capacitor voltage, v_c, can track the DC component of the MG voltage, v_{dc}, the tracking function, $P_{AS3}(s)$, is plotted in Fig. 11(c). This plot exhibits unity gain in the low-frequency regime, thereby ensuring that v_c can track v_{dc}.

The above analysis was carried out for the full-load operating point when the Group 3 converters were handling a load of 900 W each such that the total load power was 1.8 kW. The impact of load variation on converter impedances is studied in Fig. 12. It can be seen that the active stabilizer can ensure stabilization at all operating points over a wide load range by reshaping the Group 1 converter impedance. Even though the small-signal-stability is guaranteed at all operating points, it is difficult to comment on the large-signal stability of the system. A non-linear stability analysis could be carried out to identify a region of attraction where the system will be globally stable. Such a non-linear analysis will be one of the topics for future work.

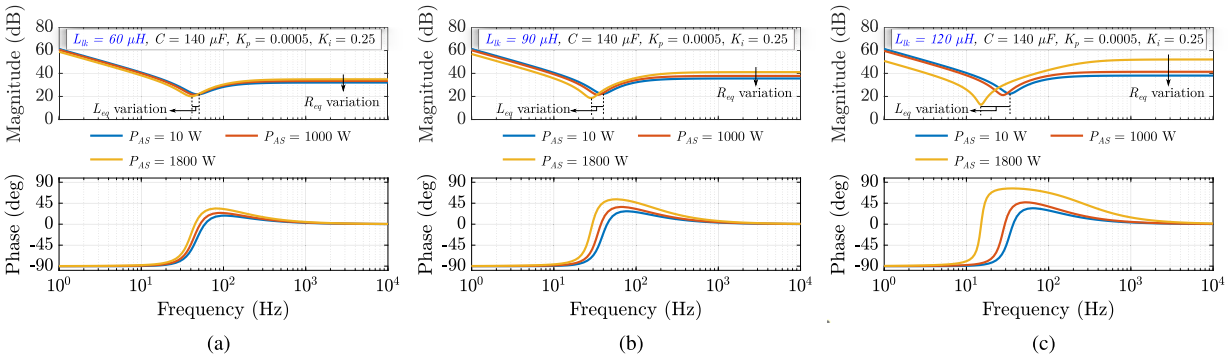

FIGURE 13. Analytical bode plots of $Z_{AS}(s)$ showcasing the effect of power transfer inductance, L_{lk}, variation.

B. ACTIVE STABILIZER PARAMETER SELECTION

This section deals with the power stage and control parameter selection for the active stabilizer used in the hardware test-bench. When a power fluctuation in the DC MG results in any DC bus voltage oscillations, the active stabilizer kicks in and helps damp out these oscillations. The peak-power rating of the active stabilizer can be chosen based on the worst-case load step in the DC MG [29]. For this work, the peak-power rating of the active stabilizer is chosen as 1.8 kW. It is to be noted that the active stabilizer does not have to handle any continuous power, and hence the cooling overhead can be minimized. The selection of the power-stage and control parameters for the active stabilizer are interlinked. The impact of parametric variation on the emulated impedance is studied to arrive at a suitable design.

1) TRANSFORMER TURNS RATIO, n

The transformer turns-ratio, n, is chosen to achieve unity-gain operation of the DAB converter-based active stabilizer to extend its soft-switching range [41]. In this work, the active stabilizer capacitor voltage, v_c, is regulated such that it tracks the DC MG voltage, v_{dc}. Hence, the turns ratio is chosen to be unity ($n = 1.0$).

2) SWITCHING FREQUENCY, $f_{sw(AS)}$

The switching frequency, $f_{sw(AS)}$ is chosen to be 50 kHz which is considerably higher than the frequency of voltage oscillations in the MG ($\approx$ 70 Hz in this case). The frequency choice also dictates the size of passive elements of the active stabilizer.

3) POWER TRANSFER INDUCTANCE, L_{lk}

The peak power, P_{pk}, that needs to be handled by the phase-shift modulated DAB converter-based active stabilizer sets the upper limit for L_{lk}.

$$L_{lk} \leq \frac{V_c V_{dc}}{8 f_{sw(AS)} P_{pk}} = 125\ \mu H \tag{20}$$

The lower limit for L_{lk} is dictated by the resolution of the digital controller platform. With a lower inductance, the required phase-shift variation to handle the peak power fluctuation is less and hence, the controller resolution becomes important. In this work, the minimum limit for L_{lk} is chosen as 60 μH. To select an appropriate value for L_{lk}, the impact of power fluctuations handled by the active stabilizer on the emulated impedance is studied. Fig. 13 showcases the effect of variation of power transfer inductance, L_{lk} on the emulated inductance, L_{eq}, and the emulated resistance, R_{eq}. It can be discerned that the impact of power fluctuations can be minimized by choosing a lower value of the inductance, L_{lk}. A lower L_{lk} of 60 μH is chosen, and L_{lk} is measured to be 64 μH in the implemented prototype.

4) POWER STAGE CAPACITANCE, C

The power stage capacitance can be selected as in [29] based on the allowable voltage ripple, ΔV_c corresponding to the peak power fluctuation handled by the active stabilizer, P_{pk}.

$$v_c = V_c + \Delta V_c\ sin(\omega t), \quad \Delta V_c < V_c \tag{21}$$

where V_c is the average DC MG voltage, ΔV_c is the amplitude of ripple in v_c, and ω is the angular frequency of the ripple in v_c (in this test-bench, $\omega \approx 2\pi \times 70\ Hz$). $\Delta V_c = 100\ V$ is assumed corresponding to the peak power of 1.8 kW.

$$C \geq \frac{P_{pk}}{V_c \Delta V_c \omega} = 136\ \mu F \tag{22}$$

Hence, a 140 μF capacitance is chosen for this work. A parametric sweep is performed to understand the impact of C on the emulated small-signal impedance. In Fig. 14(a), the emulated impedance, $Z_{AS}(s)$ is plotted when the active stabilizer capacitance, C, is varied. Varying the power stage capacitance, C is equivalent to varying the emulated capacitance, C_{eq}, since $C_{eq} = C$. The effect of C_{eq} is dominant in the low-frequency regime until the $L_{eq}C_{eq}$ resonance. A higher capacitance lowers the impedance magnitude in the lower frequency regime, and it also shifts the resonant frequency to the left.

5) CONTROLLER PARAMETERS, K_p AND K_i

K_p and K_i are selected based on (19) to emulate a desired R_{eq} and L_{eq}.

In Fig. 14(b), the emulated impedance, $Z_{AS}(s)$ is plotted when the proportional gain of the controller, K_p, is varied.

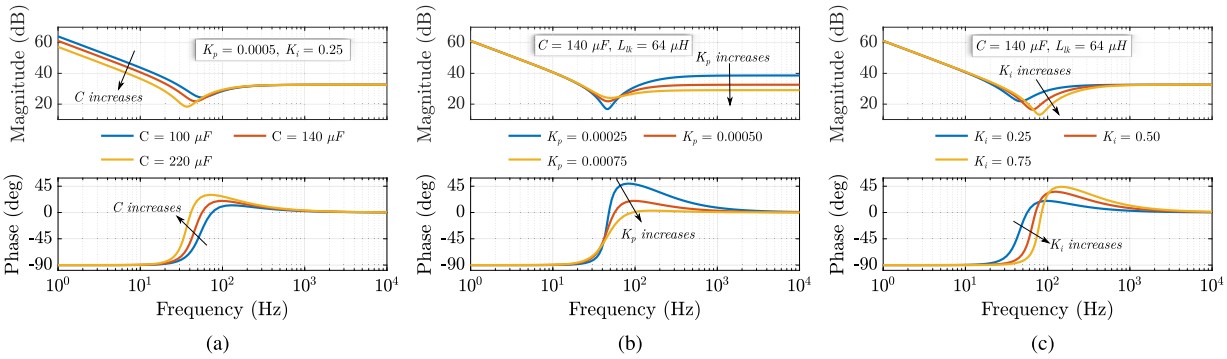

FIGURE 14. Analytical bode plots of $Z_{AS}(s)$ showcasing (a) effect of power stage capacitance, C, variation (b) effect of K_p variation and (c) effect of K_i variation.

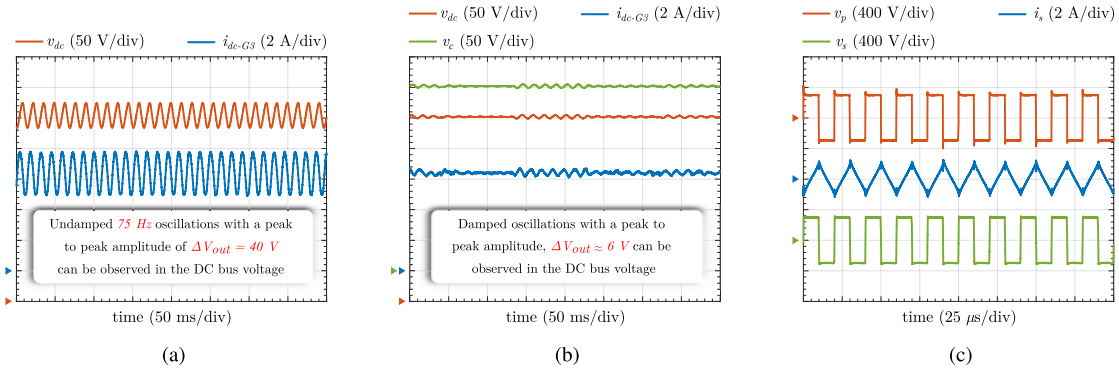

FIGURE 15. Experimental plots showcasing (a) DC voltage instability in the microgrid (b) Stabilizing effect due to the addition of proposed active stabilizer (c) Steady-state waveforms from DAB converter based active stabilzer converter. A digital noise filter (with 40 kHz cut-off frequency) is used while capturing the waveforms in (a) and (b) using a Lecroy HDO6104 oscilloscope.

From (19), it is evident that a change in K_p will affect the emulated resistance, R_{eq}. Hence, its effect is dominant in the high-frequency regime. A higher K_p lowers the impedance magnitude in the higher frequency regime (by emulating a lower R_{eq}) while simultaneously improving the damping of the resonant circuit.

The damping resistance, R_{eq}, should be chosen such that the active stabilizer mitigates the negative incremental impedance effect due to Group 1 and Group 3 converters in the DC MG.

$$R_{eq} \leq min\left\{\frac{V_{dc}^2}{P_{G1}}, \frac{V_{dc}^2}{P_{G3}}\right\}, \quad K_p = \frac{1}{R_{eq}\lambda V_{dc}} \tag{23}$$

where P_{G1} is the combined power rating of all the converters that belong to Group 1 and P_{G3} is the combined power rating of all the converters that belong to Group 3. For the experimental test-bench, $P_{G1} = P_{G3} = 1.8\ kW$.

In Fig. 14(c), the emulated impedance, $Z_{AS}(s)$ is plotted when the integral gain of the controller, K_i, is varied. A change in K_i will affect the emulated inductance, L_{eq}, as per (19). A higher K_i lowers the emulated inductance, L_{eq}, thereby shifting the resonant frequency to the right. L_{eq} is chosen such that the resonant frequency, ω_r, of the emulated small-signal impedance is slightly lower than the frequency where the undesirable impedance interaction is observed, ω. In this test-bench, $\omega \approx 70$ Hz as seen in Fig. 11(a).

$$L_{eq} = \frac{1}{\omega_r^2 C_{eq}}, \quad \omega_r \leq \omega, \quad K_i = \frac{1}{L_{eq}\lambda V_{dc}} \tag{24}$$

In this work, ω_r is chosen to be 45 Hz. Such a design ensures that the active stabilizer will offer sufficient damping while improving the overall phase-margin to stabilize the DC MG.

VI. RESULTS AND DISCUSSION

The effectiveness of the proposed solution is validated using hardware-based experiments in the laboratory DC MG test bench under both steady-state and transient conditions.

A. STEADY-STATE TESTS

Steady-state experimental test results are shown in Fig. 15. The experiments correspond to the operating condition wherein Group 1 converter is trying to regulate the DC MG voltage, v_{dc} to 300 V, and Group 3 converters are drawing a power of about 1.8 kW from the MG. The DC MG voltage, v_{dc}, and the DC current drawn by the Group 3 converters, i_{dc-G3} are shown in Fig. 15(a). As expected from analysis, $\approx$ 75 Hz oscillations are observed in the experimental waveforms. The slight difference in the frequency of oscillations between experimental results and analytical models is attributed to (i) the passive component tolerances within the

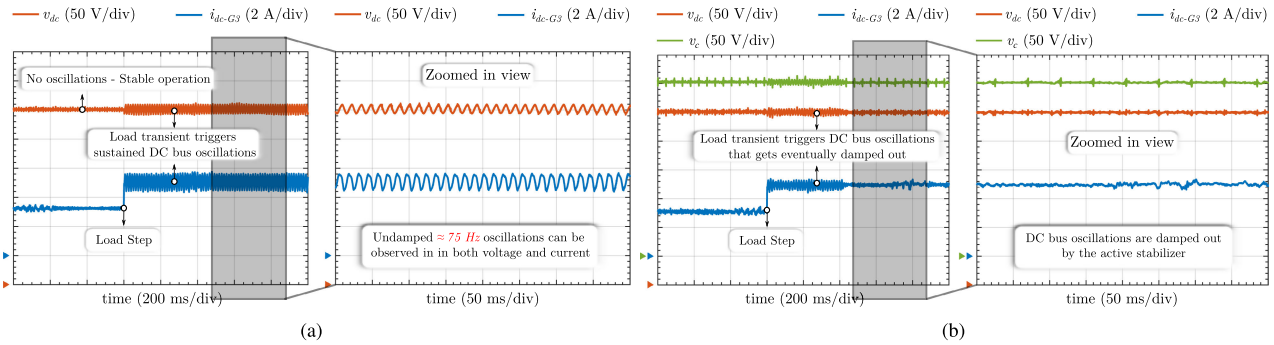

FIGURE 16. Experimental plots are showcasing a load transient (a) without active stabilizer (b) with the addition of the proposed active stabilizer.

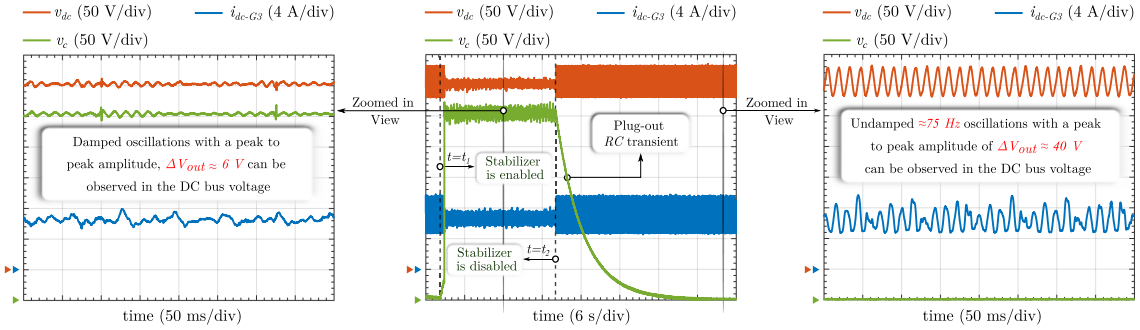

FIGURE 17. Experimental plot showcasing active stabilizer plug-in and plug-out transients.

overall DC microgrid system (ii) unaccounted losses within the converters (such as the semiconductor losses and losses in passive components) leading to a slight shift in operating point. The active stabilizer is now introduced, and the captured results are shown in Fig. 15(b). It can be seen that the proposed solution considerably improves the system stability margins. The active stabilizer capacitor voltage, v_c follows the MG DC voltage, v_{dc}. The steady-state waveforms from the active stabilizer DAB converter are captured in Fig. 15(c). The operating phase-shift between the bridge voltages, v_p and v_s, is nearly zero, indicating no significant active power exchange between the active stabilizer and the DC MG. Further, the high-frequency DAB converter current's triangular nature, i_s, indicates that the DAB current comprises mostly the magnetizing current component drawn by the transformer. The active stabilizer consumes a very minimal amount of active power from the DC MG to meet its losses. As the DAB converter does not handle any active power under steady-state conditions, the efficiency of the DAB converter-based active stabilizer would have minimal impact on the system. Hence, the conventional single phase-shift scheme was adopted for the DAB converter-based active stabilizer for simplicity.

B. LOAD TRANSIENTS

In a practical DC MG, sudden changes in load can commonly occur as and when a load is plugged in or plugged out. Hence, it is important to assess the performance of the active stabilizer under such transients. In this set of experiments, the effect of load transients on DC MG stability is studied with and without the active stabilizer. In these experiments, Group 1 converter is trying to regulate the DC MG voltage, v_{dc} to 300 V while Group 3 converters introduce a step-change in load (900 W to 1500 W). It can be seen from Fig. 16(a) that the step change in load triggers undamped ≈ 75 Hz oscillations in the DC bus without the proposed stabilizer. The experiment is repeated with the proposed active stabilizer, and the results are captured in Fig. 16(b). The active stabilizer effectively damps out the oscillations in the DC bus as predicted by the small-signal models for various loading conditions as in Fig. 12. The small-signal impedance plots in Fig. 12 reveal useful information about the local stability around each load point in the trajectory and the frequency of oscillations.

C. PLUG-IN AND PLUG-OUT TRANSIENTS

In this experiment, Group 1 converter is trying to regulate the DC MG voltage, v_{dc} to 300 V, and Group 3 converters are drawing a power of about 1.8 kW from the MG. Undamped oscillations at $\approx$ 75 Hz can be observed in Fig. 17 till time, $t < t_1$. The active stabilizer is inactive in this time period. At time instant, $t = t_1$, the active stabilizer is dynamically plugged in. It is observed that the DC bus oscillations are damped out by the active stabilizer as soon as the capacitor voltage, v_c, starts tracking the DC MG voltage. At time instant, $t = t_2$, the active stabilizer is plugged out. The DC MG voltage reverts to its original state as indicated by the recurrence of $\approx$ 75 Hz undamped oscillations. The active stabilizer capacitor voltage, v_c, gets discharged by a bleeder resistance that is connected in parallel with the active stabilizer capacitor, C. While the steady-state behavior (when $v_c = v_{dc}$) can be explained by the small-signal model based

analysis presented, a non-linear large-signal model based analysis could reveal insights about the global stability during such transients. Such a large-signal analysis will be one of the topics for future work.

VII. CONCLUSION

A grouping methodology is presented to categorize the converters in a typical DC MG. The proposed grouping methodology is used to derive an intuitive small-signal model for the DC MG without using the power-stage or the control parameters of individual converters. Since the converters in some DC MG applications could be commercial-off-the-shelf installations with limited flexibility and access for controller auto-tuning, a hardware-based active voltage stabilizer with inherent galvanic isolation is proposed to stabilize the system.

System stability is achieved by emulating an *RLC* type small-signal impedance across the DC bus using the active stabilizer and its associated control strategy. The proposed strategy helps prevent undesirable impedance interactions within the system by improving the system stability margins. Further, the active stabilizer handles the power fluctuations during transients. The proposed DAB converter-based active stabilizer concept is experimentally validated using a DC MG test-bench. As the active stabilizer is not rated to handle any continuous power, the cooling overhead can be minimized, potentially leading to highly power dense solutions. While it is demonstrated that the active stabilizer can damp out oscillations and stabilize the DC MG during steady-state and transient operating conditions, a large-signal stability analysis could reveal additional insights about the operation and global stability of the active stabilizer. It will be evaluated in our future work. Another focus of our future work will be to modify the hardware test-bench to facilitate bidirectional power exchange between the DC MG and the AC grid.

REFERENCES

[1] B. Nordman and K. Christensen, "DC local power distribution: Technology, deployment, and pathways to success," *IEEE Electrific. Mag.*, vol. 4, no. 2, pp. 29–36, Jun. 2016.

[2] G. Buticchi, L. Costa, and M. Liserre, "Improving system efficiency for the more electric aircraft: A look at DCDC converters for the avionic onboard DC microgrid," *IEEE Ind. Electron. Mag.*, vol. 11, no. 3, pp. 26–36, Sep. 2017.

[3] Z. Jin, G. Sulligoi, R. Cuzner, L. Meng, J. C. Vasquez, and J. M. Guerrero, "Next-generation shipboard DC power system: Introduction smart grid and DC microgrid technologies into maritime electrical netowrks," *IEEE Electrific. Mag.*, vol. 4, no. 2, pp. 45–57, Jun. 2016.

[4] I. Aharon and A. Kuperman, "Topological overview of powertrains for battery-powered vehicles with range extenders," *IEEE Trans. Power Electron.*, vol. 26, no. 3, pp. 868–876, Mar. 2011.

[5] A. P. N. Tahim, D. J. Pagano, E. Lenz, and V. Stramosk, "Modeling and stability analysis of islanded DC microgrids under droop control," *IEEE Trans. Power Electron.*, vol. 30, no. 8, pp. 4597–4607, Aug. 2015.

[6] H. Liu, W. Guo, D. Cheng, Y. Wang, and M. Wang, "Stability and bifurcation analysis of DC microgrid with multiple droop control sources and loads," *IEEE Trans. Power Electron.*, vol. 36, no. 2, pp. 2361–2372, Feb. 2021.

[7] A. Riccobono and E. Santi, "Comprehensive review of stability criteria for DC power distribution systems," *IEEE Trans. Ind. Appl.*, vol. 50, no. 5, pp. 3525–3535, Sep. 2014.

[8] C. M. Wildrick, F. C. Lee, B. H. Cho, and B. Choi, "A method of defining the load impedance specification for a stable distributed power system," *IEEE Trans. Power Electron.*, vol. 10, no. 3, pp. 280–285, May 1995.

[9] X. Feng, J. Liu, and F. C. Lee, "Impedance specifications for stable DC distributed power systems," *IEEE Trans. Power Electron.*, vol. 17, no. 2, pp. 157–162, Mar. 2002.

[10] Z. Huang, S. Wong, and C. K. Tse, "Revisiting stability criteria for DC power distribution systems based on power balance," *CPSS Trans. Power Electron. Appl.*, vol. 2, no. 1, pp. 76–85, Apr. 2017.

[11] X. Zhang, X. Ruan, and C. K. Tse, "Impedance-based local stability criterion for DC distributed power systems," *IEEE Trans. Circuits Syst. I, Reg. Papers*, vol. 62, no. 3, pp. 916–925, Mar. 2015.

[12] A. M. Rahimi and A. Emadi, "Active damping in DC/DC power electronic converters: A novel method to overcome the problems of constant power loads," *IEEE Trans. Ind. Electron.*, vol. 56, no. 5, pp. 1428–1439, May 2009.

[13] A. Kwasinski and C. N. Onwuchekwa, "Dynamic behavior and stabilization of DC microgrids with instantaneous constant-power loads," *IEEE Trans. Power Electron.*, vol. 26, no. 3, pp. 822–834, Mar. 2011.

[14] V. M. Iyer, S. Gulur, and S. Bhattacharya, "Small-signal stability assessment and active stabilization of a bidirectional battery charger," *IEEE Trans. Ind. Appl.*, vol. 55, no. 1, pp. 563–574, Jan. 2019.

[15] A. A. A. Radwan and Y. A.-R.-I. Mohamed, "Linear active stabilization of converter-dominated DC microgrids," *IEEE Trans. Smart Grid*, vol. 3, no. 1, pp. 203–216, Mar. 2012.

[16] R. Ahmadi and M. Ferdowsi, "Improving the performance of a line regulating converter in a converter-dominated DC microgrid system," *IEEE Trans. Smart Grid*, vol. 5, no. 5, pp. 2553–2563, Sep. 2014.

[17] M. Karbalaye Zadeh, R. Gavagsaz-Ghoachani, S. Pierfederici, B. Nahid-Mobarakeh, and M. Molinas, "Stability analysis and dynamic performance evaluation of a power electronics-based DC distribution system with active stabilizer," *IEEE J. Emerg. Sel. Topics Power Electron.*, vol. 4, no. 1, pp. 93–102, Mar. 2016.

[18] A. Aldhaheri and A. H. Etemadi, "Stabilization and performance preservation of DC–DC cascaded systems by diminishing output impedance magnitude," *IEEE Trans. Ind. Appl.*, vol. 54, no. 2, pp. 1481–1489, Apr. 2018.

[19] H. Abdollahi, S. Arrua, T. Roinila, and E. Santi, "A novel DC power distribution system stabilization method based on adaptive resonance-enhanced voltage controller," *IEEE Trans. Ind. Electron.*, vol. 66, no. 7, pp. 5653–5662, Jul. 2019.

[20] P. Magne, B. Nahid-Mobarakeh, and S. Pierfederici, "General active global stabilization of multiloads DC-power networks," *IEEE Trans. Power Electron.*, vol. 27, no. 4, pp. 1788–1798, Apr. 2012.

[21] P. Magne, B. Nahid-Mobarakeh, and S. Pierfederici, "Active stabilization of DC microgrids without remote sensors for more electric aircraft," *IEEE Trans. Ind. Appl.*, vol. 49, no. 5, pp. 2352–2360, Sep. 2013.

[22] R. Hassan, H. Wang, and R. Zane, "Continuous stability monitoring of DC microgrids using controlled injection," in *Proc. IEEE Appl. Power Electron. Conf. Expo. (APEC)*, Mar. 2019, pp. 1357–1364.

[23] J. Morroni, R. Zane, and D. Maksimovic, "Design and implementation of an adaptive tuning system based on desired phase margin for digitally controlled DC–DC converters," *IEEE Trans. Power Electron.*, vol. 24, no. 2, pp. 559–564, Feb. 2009.

[24] A. Khodamoradi, G. Liu, P. Mattavelli, T. Caldognetto, and P. Magnone, "Analysis of an online stability monitoring approach for DC microgrid power converters," *IEEE Trans. Power Electron.*, vol. 34, no. 5, pp. 4794–4806, May 2019.

[25] A. Riccobono, M. Cupelli, A. Monti, E. Santi, T. Roinila, H. Abdollahi, S. Arrua, and R. A. Dougal, "Stability of shipboard DC power distribution: Online impedance-based systems methods," *IEEE Electrific. Mag.*, vol. 5, no. 3, pp. 55–67, Sep. 2017.

[26] K.-T. Mok, M.-H. Wang, S.-C. Tan, and S. Y. R. Hui, "DC electric springs—A technology for stabilizing DC power distribution systems," *IEEE Trans. Power Electron.*, vol. 32, no. 2, pp. 1088–1105, Feb. 2017.

[27] A. Hosseinipour and H. Hojabri, "Small-signal stability analysis and active damping control of DC microgrids integrated with distributed electric springs," *IEEE Trans. Smart Grid*, vol. 11, no. 5, pp. 3737–3747, Sep. 2020.

[28] K. A. Potty, E. Bauer, H. Li, and J. Wang, "Smart resistor: Stabilization of DC microgrids containing constant power loads using high-bandwidth power converters and energy storage," *IEEE Trans. Power Electron.*, vol. 35, no. 1, pp. 957–967, Jan. 2020.

[29] X. Zhang, X. Ruan, H. Kim, and C. K. Tse, "Adaptive active capacitor converter for improving stability of cascaded DC power supply system," *IEEE Trans. Power Electron.*, vol. 28, no. 4, pp. 1807–1816, Apr. 2013.
[30] V. M. Iyer, S. Gulur, S. Bhattacharya, J. Kikuchi, S. Sridharan, K. Zou, and C. Chen, "An active voltage stabilizer for a generic DC microgrid," in *Proc. IEEE Energy Convers. Congr. Expo. (ECCE)*, Sep. 2019, pp. 462–468.
[31] T. Suntio and D. Gadoura, "Use of unterminated two-port modeling technique in analysis of input filter interactions in telecom DPS systems," in *Proc. 24th Annu. Int. Telecommun. Energy Conf.*, Sep. 2002, pp. 560–565.
[32] I. Cvetkovic, D. Boroyevich, P. Mattavelli, F. C. Lee, and D. Dong, "Unterminated small-signal behavioral model of DC–DC converters," *IEEE Trans. Power Electron.*, vol. 28, no. 4, pp. 1870–1879, Apr. 2013.
[33] R. W. Erickson and D. Maksimovic, *Fundamentals of Power Electronics*, 2nd ed. Norwell, MA, USA: Kluwer, 2004.
[34] N. Nise, *Control Systems Engineering*. Hoboken, NJ, USA: Wiley, 2000.
[35] R. W. A. A. De Doncker, D. M. Divan, and M. H. Kheraluwala, "A three-phase soft-switched high-power-density DC/DC converter for high-power applications," *IEEE Trans. Ind. Appl.*, vol. 27, no. 1, pp. 63–73, Feb. 1991.
[36] M. N. Kheraluwala, R. W. Gascoigne, D. M. Divan, and E. D. Baumann, "Performance characterization of a high-power dual active bridge DC-to-DC converter," *IEEE Trans. Ind. Appl.*, vol. 28, no. 6, pp. 1294–1301, Nov. 1992.
[37] S. S. Shah, V. M. Iyer, and S. Bhattacharya, "Exact solution of ZVS boundaries and AC-port currents in dual active bridge type DC–DC converters," *IEEE Trans. Power Electron.*, vol. 34, no. 6, pp. 5043–5047, Jun. 2019.
[38] *Low-Voltage Electrical Installations—Part 1: Fundamental Principles, Assessment of General Characteristics, Definitions*, Standard 60364-1:2005, Nov. 2005, pp. 1–79.
[39] V. M. Iyer, S. Gulur, G. Gohil, and S. Bhattacharya, "An approach towards extreme fast charging station power delivery for electric vehicles with partial power processing," *IEEE Trans. Ind. Electron.*, vol. 67, no. 10, pp. 8076–8087, Oct. 2020.
[40] (2021). *Plexim: Electrical Engineering Software*. Accessed: May 15, 2021. [Online]. Available: https://www.plexim.com/
[41] V. M. Iyer, S. Gulur, and S. Bhattacharya, "Optimal design methodology for dual active bridge converter under wide voltage variation," in *Proc. IEEE Transp. Electrific. Conf. Expo (ITEC)*, Jun. 2017, pp. 413–420.

VISHNU MAHADEVA IYER (Senior Member, IEEE) received the B.Tech. degree in electrical and electronics engineering from the College of Engineering, Trivandrum, India, in 2011, the M.E. degree in electrical engineering from the Indian Institute of Science (IISc), Bengaluru, India, in 2013, and the Ph.D. degree in electrical engineering from North Carolina State University, Raleigh, NC, USA, in 2020. He worked as a Lead Engineer with GE Research, Niskayuna, USA, in 2020, and as a Power Electronics Engineer with GE Research, Bengaluru, from 2013 to 2015. He is currently working as an Assistant Professor at the IISc.

SRINIVAS GULUR (Member, IEEE) received the B.E. degree in electrical and electronics engineering from Anna University, India, in 2010, the M.S. degree in electrical engineering systems from the University of Michigan, Ann Arbor, MI, USA, in 2013, and the Ph.D. degree in electrical engineering from North Carolina State University, Raleigh, NC, USA, in 2020. He worked with the Power Electronics Group, Indian Institute of Science (IISc), Bengaluru, India, from 2013 to 2015. He is currently working as a Senior Power Electronics Engineer at Lucid Motors Inc., Newark, CA, USA.

SUBHASHISH BHATTACHARYA (Senior Member, IEEE) received the B.E. degree from the Indian Institute of Technology Roorkee, Roorkee, India, the M.E. degree from the Indian Institute of Science, Bengaluru, India, and the Ph.D. degree from the University of Wisconsin-Madison, Madison, WI, USA, in 2003, all in electrical engineering.

He was with the FACTS and Power Quality Division, Westinghouse/Siemens Power T&D, from 1998 to 2005. In August 2005, he joined with North Carolina State University, Raleigh, NC, USA, where he is currently the Duke Energy Distinguished Professor of electrical and computer engineering. He is a Founding Faculty Member with the NSF FREEDM Systems Center, DOE Power America Institute. His Ph.D. degree research on active power filters was commercialized by York Corporation for air-conditioner chillers. His research interests include solid-state transformers, MV power converters, FACTS, utility applications, high-frequency magnetics, and power conversion applications of SiC devices.

JUN KIKUCHI (Member, IEEE) received the M.S. and Ph.D. degrees in electrical engineering, the M.A. degree in mathematics from the University of Wisconsin-Madison, Madison, WI, USA, in 1999, 2002, and 2004, respectively, and the M.S. degree in marine engineering from the Kobe Mercantile Marine Academy, Japan, in 1984. He has been working with the Ford Motor Company, Research and Innovation Center, since 2007. He has worked with Mitsubishi Electric Corporation, Kobe Mercantile Marine Academy, and Eaton Corporation.

SRIKANTHAN SRIDHARAN received the bachelor's degree in electrical and electronics engineering from the College of Engineering, Anna University, Chennai, India, in 2006, the master's degree in electrical engineering from the Indian Institute of Technology Madras, India, in 2009, and the Ph.D. degree in electrical engineering from the University of Illinois, Urbana–Champaign, USA, in 2015.

He is currently working as an Assistant Professor with the Department of Engineering Design, IIT Madras. He has been with Ford Motor Company, Siemens Corporate Technology, and GE Global Research Center. His research interests include power electronics, machines and drives control, and electric transportation.

KE ZOU received the B.S. and M.S. degrees from Xi'an Jiaotong University, China, in 2005 and 2008, respectively, and the Ph.D. degree from The Ohio State University, USA, in 2012. He is currently with Ford Motor Company, Dearborn, MI, USA. His research interests include the design of traction drive inverters in hybrid electric vehicles (HEV), on-board and off-board chargers, and the characterization of power semiconductor devices.

CHINGCHI CHEN received the Ph.D. degree in electrical engineering from the University of Wisconsin-Madison, in 1994. He has been with the Ford Research and Advanced Engineering, leading power electronics research for on-vehicle applications. He has been working on various areas in power electronics for automotive applications, including topology evaluation, dynamic analysis, reliability assessment, WBG technology evaluation, and package design.